Atmos. Chem. Phys. Discuss., 15, 33731–33754, 2015
www.atmos-chem-phys-discuss.net/15/33731/2015/
doi:10.5194/acpd-15-33731-2015

Atmospheric Chemistry and Physics Discussions

Vortex-wide chlorine activation by a mesoscale PSC event in the Arctic winter of 2009/10

T. Wegner[1], M. C. Pitts[1], L. R. Poole[2], I. Tritscher[3], J.-U. Grooß[3], and H. Nakajima[4]

[1]Chemistry and Dynamics Branch – Langley Research Center, National Aeronautics and Space Administration, Hampton, Virginia, USA
[2]Science Systems and Applications, Hampton, Virginia, USA
[3]Institute for Energy and Climate Research IEK-7, Forschungszentrum Jülich, Jülich, Germany
[4]National Institute for Environmental Studies, Tsukuba, 305-8506, Japan

Received: 22 October 2015 – Accepted: 11 November 2015 – Published: 30 November 2015

Correspondence to: T. Wegner (tobias.wegner@nasa.gov)

Published by Copernicus Publications on behalf of the European Geosciences Union.

Abstract

In the Arctic polar vortex of the 2009/10 winter temperatures were low enough to allow widespread formation of Polar Stratospheric Clouds (PSC). These clouds occurred during the initial chlorine activation phase which provided the opportunity to investigate the impact of PSCs on chlorine activation. Satellite observations of gas-phase species and PSCs are used in combination with trajectory modeling to assess this initial activation. The initial activation occurred in association with the formation of PSCs over the east coast of Greenland at the beginning of January 2010. Although this area of PSCs covered only a small portion of the vortex, it was responsible for almost the entire initial activation of chlorine vortex wide. Observations show HCl mixing ratios decreased rapidly in and downstream of this region. Trajectory calculations and simplified heterogeneous chemistry modeling confirmed that the initial chlorine activation continued until $ClONO_2$ was completely depleted and the activated air masses were advected throughout the polar vortex. For the calculation of heterogeneous reaction rates, surface area density is estimated from backscatter observations. Modeled heterogeneous reaction rates along trajectories intersecting with the PSC indicate that the initial phase of chlorine activation occurred in just a few hours. These calculations also indicate that chlorine activation on the binary background aerosol is significantly slower than on the PSCs and the observed chlorine activation can only be explained by an increase in surface area density due to PSCs. Furthermore, there is a strong correlation between the magnitude of the observed HCl depletion and PSC surface area.

1 Introduction

Heterogeneous chemistry on stratospheric aerosol and Polar Stratospheric Clouds (PSCs) plays a crucial role in the formation of the ozone hole (Solomon, 1999). While the stratospheric aerosol layer is present globally at all times (Junge et al., 1961), PSCs only form over the polar regions of the winter hemisphere (Lowe and MacKenzie, 2008).

ACPD
15, 33731–33754, 2015

PSCs are ubiquitous in the Antarctic winter but wide-spread PSC occurrence over the Arctic is only observed during very cold winters (Pitts et al., 2009, 2011). PSCs have a substantial influence on the chemical composition of the polar stratosphere. Heterogeneous chemistry on such particles impacts chlorine species (Solomon et al., 1986) and PSC particles can grow large enough to effectively denitrify (Fahey et al., 2001) and dehydrate (Kelly et al., 1989) the lower stratosphere. Although PSCs have a pivotal role in determining stratospheric chemical composition and have been subject to extensive research since the 1980s, some details are still subject to uncertainty.

One of the key questions is to what extent is heterogeneous chemistry on PSCs responsible for converting inorganic chlorine species to photo-active species (chlorine activation) on a vortex-wide scale and what are the time-scales for this processing. Several studies (e.g. Drdla and Müller, 2012; Wohltmann et al., 2013; Kirner et al., 2015) have suggested that the influence of PSCs on chlorine activation is subordinate to that due to cold binary aerosol on a vortex-wide scale. When temperatures approach the frost point, heterogeneous reaction rates are large enough to activate chlorine on time-scales of minutes to hours regardless of surface type (Wegner et al., 2012). On the other hand, Carslaw et al. (1998) and Kühl et al. (2004) showed that nearly complete chlorine activation can be achieved in a mountain-wave PSC at sufficiently low temperatures and large surface area densities.

This study investigates the influence of mesoscale PSCs on the chemical composition of the entire vortex. Mesoscale PSCs are larger in spatial scale than mountain-wave induced PSCs but still only cover a small fraction of the polar vortex. We use data from the space-borne lidar CALIOP (Cloud-Aerosol LIdar with Orthogonal Polarization) instrument for studying PSCs and data from the Microwave Limb Sounder (MLS) in combination with chemistry transport model calculations to examine the impact of a mesoscale PSC on the chemical composition of the Arctic vortex in January 2010. CALIOP backscatter observations are used to derive particle surface area density (SAD) which is then used to calculate chlorine activation. Through these anal-

ACPD
15, 33731–33754, 2015

yses, we will examine the impact of PSC SAD enhancements on chlorine activation compared with the cold binary background aerosol.

2 Instrumentation and model description

The CALIPSO (Cloud-Aerosol Lidar and Infrared Pathfinder Spaceborne Observations) satellite is member of the A-train satellite constellation (Stephens et al., 2002) orbiting at an inclination of 98.2° that provides coverage up to 82° latitude in each hemisphere. Its primary instrument is CALIOP which measures backscatter at 1064 and 532 nm, with the 532 nm channel separated into orthogonal polarization components parallel and perpendicular to the polarization plane of the outgoing laser beam (Winker et al., 2009). Details about the CALIOP PSC classification algorithm can be found in Pitts et al. (2009, 2011, 2013). The CALIOP classification scheme distinguishes between Supercooled Ternary Solutions (STS), mixtures of STS and Nitric Acid Trihydrate (NAT) and ice. Mixtures of STS and NAT are further divided into MIX 1, MIX 2 and MIX 2 enhanced where NAT number density increases from MIX 1 to MIX 2 enhanced. CALIOP also distinguishes between synoptic and wave ice.

The Microwave Limb Sounder (MLS) is an instrument on the EOS (Earth Observing System) Aura satellite, which is also part of the A-train constellation and has provided nearly continuous measurements since 2004 (Waters et al., 2006). MLS provides about 3500 profiles of gas-phase species and temperature from Earth's surface to 90 km altitude between 82° N and 82° S per day. In this study, we use MLS HCl data from retrieval version 3.3 (Livesey et al., 2011) which is comparable to version 2.2. Retrieval version 2.2 for HCl has been validated in Santee et al. (2008). The vertical resolution and precision of the HCl observations are 3 km and 0.2–0.3 ppbv, respectively.

CALIOP and MLS observations are linearly interpolated to a 20° by 2° (longitude × latitude) grid on fixed potential temperature surfaces each day. Potential temperature is calculated from the native MLS pressure levels and temperature data from

ACPD
15, 33731–33754, 2015

the Modern-Era Retrospective Analysis for Research and Applications (MERRA, Rienecker et al., 2011).

Air mass trajectories are calculated with the Chemical Lagrangian Model of the Stratosphere (CLaMS) which uses a fourth-order Runge–Kutta scheme (McKenna et al., 2002). The wind fields for these trajectories are taken from ERA-INTERIM (Dee et al., 2011). Threshold temperatures T_{NAT} (NAT, nitric acid trihydrate, existence temperature) and T_{ACl} (chlorine activation temperature) which can serve as indicators for chlorine activation (Drdla and Müller, 2012) are calculated with temperatures and trace gas concentration from a CLaMS simulation described in Grooß et al. (2014). The vortex edge is defined according to Nash et al. (1996).

A simple algorithm was defined to determine the locations of air masses that had previously passed through the PSC event. Trajectories are used to track air masses downwind of a PSC that is defined by the CALIOP detection threshold. These air masses are called "Processed Air" since we assume that chlorine activation predominantly occurred in such air masses. On a given day a grid box is labeled as filled with "Processed Air" if a processed air mass has passed through this grid box on that day. A grid box is then labeled as filled with "Unprocessed Air" if on a given day no processed air masses have passed through this grid box even if this grid box was marked with "Processed Air" on previous days. This way we can describe for each day the fraction of the vortex that is filled with air masses which have previously encountered a PSC.

PSCs are identified in the CALIOP measurements as enhancements in backscatter with an altitude dependent threshold of β_{532} between 2 and 4×10^{-5} km^{-1} sr^{-1} in the algorithm described in Pitts et al. (2013). We show sensitivity studies that use different threshold backscatter ratios between 3×10^{-5} and 1.5×10^{-4} km^{-1} sr^{-1}, where the latter backscatter threshold is high enough to indicate the presence of ice PSCs.

For a realistic determination of heterogeneous reaction rates, an estimation of the particle surface area density (SAD) as realistic as possible is necessary. Following the approach of Gobbi (1995), we performed Mie calculations for unimodal lognormal particle size distributions representative of the polar stratosphere to derive a rela-

ACPD
15, 33731–33754, 2015

tionship for estimating liquid particle SAD from CALIOP measurements of particulate backscatter at 532 nm. Figure 1a shows calculated liquid particle SAD and backscatter ($\beta_{532,liquid}$) as a function of temperature relative to the frost point ($T - T_{frost}$) for the following conditions: pressure = 30 hPa, HNO_3 = 15 ppbv, H_2O = 5 ppmv, particle number density $N = 10\,cm^{-3}$ (Curtius et al., 2005), and lognormal geometric standard deviation $\sigma = 1.6$ (Lambert et al., 2012). For these calculations, liquid particle volume was prescribed as a function of temperature according to Carslaw et al. (1995); mode radius (for the Mie calculations) and SAD were then calculated from particle volume using standard relationships for a unimodal lognormal.

Calculated values of liquid SAD and $\beta_{532,liquid}$ from Fig. 1a are plotted against each other in Fig. 1b. The dashed curve shows the least-squares quadratic fit in log-log space between the two parameters, which we will use in this study. With fixed $N = 10\,cm^{-3}$ and $\sigma = 1.6$, computed points fall along the same least-squares curve for different pressure levels (50 and 70 hPa), HNO_3 mixing ratios (2, 5, and 10 ppbv), and H_2O mixing ratio (2 ppmv). Values computed for different values of N (5 and $15\,cm^{-3}$) and σ (1.3 and 1.8) fall along different curves, but all points lie within the limits depicted by the solid gray curves. Given the small envelope defined by those parameters the relationship between SAD and $\beta_{532,liquid}$ is robust and valid for the entire season. Measured values of $\beta_{532,liquid}$ larger than 3 to $5 \times 10^{-4}\,km^{-1}\,sr^{-1}$ likely signify ice PSCs. The SAD estimated using the least-squares relationship for liquid particles can be considered a lower limit of SAD for ice PSCs. The relationship between backscatter and surface area density for STS particles can then be described by:

$$\log_{10}(SAD) = 3.474 + 0.671 \cdot \log_{10}(\beta_{532}) + 0.007 \cdot \log_{10}(\beta_{532})^2 \quad (1)$$

3 The mesoscale PSC event

In December 2009, CALIOP observed an increase in backscatter over Greenland, corresponding to the first major formation of liquid/ice PSCs (Pitts et al., 2011) during the

ACPD
15, 33731–33754, 2015

Arctic winter 2009/10. The increase in SAD indicates condensation of HNO_3 on the background aerosol or the nucleation of NAT and ice particles. The PSC backscatter and areal extent increased during the following two days reaching a maximum on 2 January 2010 before slowly decreasing on subsequent days. Figure 2 shows the PSC classification according to Pitts et al. (2011) from the CALIOP observations on 2 January. The PSC extends between 20–25 km in altitude and is a mixture of all PSC types. CALIOP observations indicate that STS forms first over the west coast of Greenland followed by wave ice formation over central Greenland. Synoptic ice and NAT mixtures occur downstream of the wave ice over eastern Greenland. Figure 2 also shows the limitations of our current observations with gaps of hundreds of kilometers between the orbits. During this PSC event, the vortex was shifted away from the pole over northeast Canada and northern Russia. The vortex remained stable during this time-frame with only limited dynamic disturbances.

Figure 3 shows backscatter over a six-day period from 31 December 2009 to 5 January 2010 and the prevailing winds. From the meteorological data we estimate the wind speed in the vicinity of the PSC to be $20\,m\,s^{-1}$ which yields a residence time of about one day for air parcels traveling through the PSC. Chlorine activation is limited by the availability of the reservoir species and will cease once either HCl or $ClONO_2$ are depleted (Portmann et al., 1996). Heterogeneous chemistry on stratospheric aerosols is primarily the conversion of HCl and $ClONO_2$ into ClO_x ($ClO + 2 \cdot Cl_2O_2$). Therefore, the observations of gas-phase HCl by MLS can serve as an indicator of heterogeneous processing where low values of HCl are indicative of air masses where inorganic chlorine has been activated. Since HCl is more abundant than $ClONO_2$ at the beginning of winter, $ClONO_2$ is the limiting component in chlorine activation (Portmann et al., 1996).

Figure 3a shows that low HCl mixing ratios are co-located with the PSCs over northern Greenland on 31 December and that HCl mixing ratios upstream of the PSC are more than twice as high compared to air exposed to the PSC. CALIOP observed backscatter values above $1.5 \times 10^{-4}\,km^{-1}\,sr^{-1}$ which corresponds to a tenfold increase of SAD relative to background conditions, or to around $10\,\mu m^2\,cm^{-3}$. During all subse-

ACPD
15, 33731–33754, 2015

quent days, HCl is always lower in the vicinity of PSCs compared to areas upstream with HCl mixing ratios decreasing to less than 0.5 ppbv during this period, about a quarter of their values in a chemically unperturbed vortex.

The low HCl mixing ratios persist downstream of the PSCs and do not decrease further, in agreement with current knowledge that chlorine activation is highly dependent on SAD, temperature and the ratio of HCl/$ClONO_2$. Model calculations indicate that $ClONO_2$ is totally depleted downstream of the PSC. Additional activation can only occur when $ClONO_2$ is regenerated (Portmann et al., 1996). $ClONO_2$ controls the total amount of chlorine that can be activated while PSCs determine the area in which activation occurs. Low HCl concentrations observed in regions where our calculations indicate only unprocessed air is present could originate from either physical mixing with processed air or averaging along the MLS field of view. We also need to stress that such trajectory calculations rely on the quality of the wind fields used and are subject to errors which are difficult to quantify.

After five days, the air which was exposed to PSCs on 31 December 2009 has completed a full circumnavigation of the vortex and re-entered the region where PSCs were present on 5 January 2010. Air which was not exposed to PSCs tends to have higher HCl mixing ratios, indicating that little chlorine activation occurred outside of PSCs, as shown clearly in the 2 January data in Fig. 3c. Air over the Barents Sea followed its own cyclonic circulation separate from the polar vortex. Air in this region did not encounter PSCs nor sunlight, leading to constant HCl mixing ratios. This situation persisted for several days and the trajectories passing through PSCs actually flowed around this region. After 3 January the air flows into the PSC covered area from the unobserved area north of 82° so we do not have a complete history of HCl concentrations in relation to PSC exposure for these air masses.

As Fig. 3 indicates, it takes about five days for air to circumnavigate the polar vortex. This means that a PSC with a sufficiently large meridional extent can activate chlorine throughout the entire vortex even when the PSC itself only covers a small fraction of the vortex. Such a PSC can serve as a “processing reactor” for chlorine activation

ACPD
15, 33731–33754, 2015

with heterogeneous chemistry basically limited to the time air masses spend inside the PSC. Vortex-averaged values which are commonly used to estimate chlorine activation would not accurately represent the true nature of activation within the vortex, under these conditions.

While chlorine activation is generally observed within the boundary of elevated backscatter values as observed by CALIOP, the lowest HCl mixing ratios are correlated with the highest backscatter values. Figure 4 shows the ratio of mean HCl mixing ratios in processed air which has been exposed to backscatter values above certain thresholds to the vortex average HCl mixing ratio. The backscatter thresholds in Fig. 4a–c indicate the formation of STS and 4d suggests the presence of ice since backscatter values of this magnitude correspond to higher surface area densities than physically possible with only the condensation of HNO_3.

The ratio of mean HCl mixing ratios to the vortex average HCl mixing ratio is also shown for air which has been exposed to temperatures below either T_{NAT} or T_{ACI}. After five days the HCl mixing ratios within processed air are indistinguishable from the vortex mean because all air within the vortex has been exposed to PSCs. As the threshold backscatter value chosen for the area describing the "processing reactors" decreases, HCl mixing ratios in air which has been exposed to PSCs gradually approaches the vortex average. This shows that chlorine activation occurs locally in the area covered by PSCs but not on a vortex wide scale.

Temperature thresholds for chlorine activation do not capture this localized effect. The air exposed to an area enclosed by a temperature threshold is always very similar to the vortex average since those areas already encompass the main part of the vortex. Therefore, neither T_{NAT} nor T_{ACI} provide realistic information on the location where chlorine activation occurs for the period considered in this study. Only thresholds based on backscatter provide this information.

In addition, Fig. 4 indicates that at the beginning of the activation phase under study, the average HCl mixing ratio in the area above a chosen backscatter threshold decreases as the backscatter threshold is increased. Since backscatter can be used

ACPD
15, 33731–33754, 2015

as a proxy for surface area density, the surface area provided by PSCs appears to have a direct affect on gas-phase HCl concentrations. While HCl mixing ratios above a backscatter threshold indicative of STS (Fig. 4a) have a minimum of 70 % of vortex average HCl mixing ratios, HCl mixing ratios above a threshold suggestive of ice PSCs (Fig. 4d) have a minimum of 50 % of the vortex average HCl mixing ratios. Therefore, chlorine activation processes visibly faster with increasing surface area density. The magnitude of chlorine activation appears to be correlated with available surface area density provided by PSCs.

The mesoscale PSC event leaves a visible mark on HCl mixing ratios. When separating the polar vortex into regions of processed and unprocessed air, we find lower HCl mixing ratios in processed air (Fig. 5) between 31 December and 9 January. Observations by MLS show that for all days between 20–25 km, HCl is lower in processed air compared to unprocessed air. However, the large uncertainties indicate that the distinction between processed and unprocessed air is difficult and that the mean values are calculated from heterogeneous air masses. Still, we see a clear trend that chlorine activation has progressed further in air masses which have been exposed to PSCs.

The analysis for Fig. 5 was repeated with T_{NAT} and T_{ACl} (not shown) as indicators for processed air. Here, processed air describes those grid boxes with temperatures less than the respective threshold temperatures and grid boxes where trajectories are present which have encountered temperatures less than the temperature thresholds in their past. Two main differences emerge. First, the daily mean mixing ratios for processed and unprocessed air are more similar, making a distinction between them difficult. Second, processed air covers the entire vortex more quickly because both temperature thresholds cover a larger area of the vortex than our PSC threshold. This leads to fewer available data points. Using either of the temperature thresholds to describe processed air does not show any significant difference between processed and unprocessed air.

ACPD
15, 33731–33754, 2015

4 Modeling heterogeneous chemistry

For a quantitative understanding of the shown HCl decrease we use the trajectories combined with a very simplified heterogeneous chemistry scheme. Using the relationship in Eq. (1), we can use CALIOP backscatter to calculate PSC SAD along trajectories passing through the maximum PSC backscatter. The trajectories are initialized with H_2O, HNO_3 and HCl from MLS observations and it is assumed that at the start of the trajectories no chlorine has been activated yet. Hence, $ClONO_2$ is initialized as the difference between total inorganic chlorine (Cl_y) and HCl with Cl_y derived from the Cl_y-N_2O tracer-tracer relationship (Grooß et al., 2002). The simplified chemistry consists of three heterogeneous reactions which are modeled along the trajectories:

$$HCl + ClONO_2 \longrightarrow Cl_2 + HNO_3 \quad \text{(R1)}$$

$$ClONO_2 + H_2O \longrightarrow HOCl + HNO_3 \quad \text{(R2)}$$

$$HCl + HOCl \longrightarrow Cl_2 + H_2O \quad \text{(R3)}$$

No additional reactions are included in the calculations since they are not relevant to assess chlorine activation on time-scales of up to one day. The uptake coefficients for all three reactions are calculated for STS even when backscatter values indicate the presence of ice. However, no difference in HCl mixing ratios is evident when the uptake coefficients for ice are used once backscatter values suggest the presence of ice PSCs.

Figure 6 shows three trajectories which encounter their backscatter maximum on three different days. The maximum backscatter suggests the presence of ice clouds on 1, 2 and 3 January; however, temperatures only decrease below the frost point for a single trajectory on 6 January.

The evolution of modeled HCl and observations shows very good agreement for the first activation phase. HCl along the trajectories deviates from the observations after a couple of days. However, chlorine activation in the first half of the trajectories can still be analyzed. A decrease in HCl coincides with an increase in surface area density and $ClONO_2$ is totally depleted after the initial activation. This confirms that

ACPD
15, 33731–33754, 2015

$ClONO_2$ is indeed the limiting factor for chlorine activation because observed HCl also does not decrease further once the model shows complete removal of $ClONO_2$. The complete removal of $ClONO_2$ also occurs before the maximum in surface area density but activation starts when SAD increases above background values. Neither observations nor modeled chemistry indicate significant chlorine activation in the absence of PSCs. In fact, when heterogeneous chemistry is only modeled on a binary sulfate aerosol (without uptake of HNO_3 as temperatures decrease) chlorine activation does not only progress slower (Fig. 6d–f) dashed lines) but also does not completely deplete $ClONO_2$. While previous studies have shown that for an entire winter season heterogeneous chemistry on cold binary aerosol is sufficient to achieve complete chlorine activation (Drdla and Müller, 2012; Wohltmann et al., 2013), in the case of a mesoscale event as described in this study PSCs activate chlorine faster than the background aerosol. The observed activation could not have occurred without the additional surface area provided by PSCs. However, Fig. 6f also shows that after five days the latest, heterogeneous chemistry on only the binary aerosol has depleted all the initially available $ClONO_2$. In agreement with Drdla and Müller (2012) the degree of chlorine activation on only the background aerosol would become indistinguishable from chlorine activation on PSCs after about 10 days, or the time it takes for an air parcel to fully circumnavigate the vortex twice.

5 Conclusions

We have analyzed CALIOP and MLS observations in combination with modeled trajectories to quantify the initial chlorine activation phase for the winter 2009/10 and constrain the spatial and temporal scales on which chlorine activation occurred. Our analysis has shown that mesoscale PSCs can have a substantial effect on chlorine chemistry throughout the polar vortex, even though the PSCs themselves only cover a small fraction of the polar vortex. A substantial decrease in HCl is observed in air masses exposed to PSCs for about 24 h. MLS observations indicate that air masses

ACPD
15, 33731–33754, 2015

with low HCl mixing ratios occur downstream of this PSC event in agreement with the trajectory calculations. The modeled trajectories provide a solid approximation of the path the air has taken after it encountered the PSC and distinguish between processed and unprocessed air masses. The average daily HCl mixing ratio in processed and unprocessed air shows substantially smaller HCl mixing ratios in processed air. We've also shown that chlorine activation in the polar vortex is not always a uniform process but can occur in mesoscale PSC "processing reactors". Heterogeneous chemistry occurs in these "processing reactors" and the air is subsequently advected and mixed throughout the vortex. Chlorine activation does not occur homogeneously throughout the vortex and HCl mixing ratios can vary significantly, especially during this initial activation phase. Therefore, a vortex average point of view does not provide an accurate representation during this phase. The trajectory calculations show that the availability of $ClONO_2$ limits the extent of chlorine activation. For the first time, CALIOP backscatter observations were utilized to estimate surface area density and model heterogeneous chemistry along trajectories. Results from these simulations are in excellent agreement with observed mixing ratios of HCl. These calculations also show that the SAD enhancements from PSCs lead to faster chlorine activation than would occur on the background aerosol. While the background aerosol could eventually activate the same amount of chlorine as the PSCs, over the time and spatial scales considered in this study, the observed rate of chlorine activation can only be explained by the additional surface area provided by PSCs. While this study focuses on the Arctic, similar conditions like the situation over Greenland in January 2010 can also occur over the Antarctic. Wave ice over the Antarctic predominantly occurs over the Antarctic peninsula; therefore, this area can also serve as a processing reactor for chlorine activation.

Acknowledgements. This work is funded under NASA's postdoctoral program administered by Oak Ridge Associated Universities. We are grateful to NASA for the MERRA meteorological analysis and EOS MLS and CALIOP teams for their high-quality data products.

ACPD
15, 33731–33754, 2015

References

Carslaw, K. S., Luo, B., and Peter, T.: An analytic expression for the composition of aqueous HNO_3-H_2SO_4 stratospheric aerosols including gas phase removal of HNO_3, Geophys. Res. Lett., 22, 1887–1880, 1995. 33736

Carslaw, K. S., Wirth, M., Luo, B. P., Dörnbrack, A., Leutbecher, M., Volkert, H., nad J. T. Bacmeister, W. R., Reimer, E., and Peter, T.: Increased stratospheric ozone depletion due to mountain-induced atmospheric waves, Nature, 391, 675–678, doi:10.1038/35589, 1998. 33733

Curtius, J., Weigel, R., Vössing, H.-J., Wernli, H., Werner, A., Volk, C.-M., Konopka, P., Krebsbach, M., Schiller, C., Roiger, A., Schlager, H., Dreiling, V., and Borrmann, S.: Observations of meteoric material and implications for aerosol nucleation in the winter Arctic lower stratosphere derived from in situ particle measurements, Atmos. Chem. Phys., 5, 3053–3069, doi:10.5194/acp-5-3053-2005, 2005. 33736

Dee, D. P., Uppala, S. M., Simmons, A. J., Berrisford, P., Poli, P., Kobayashi, S., Andrae, U., Balmaseda, M. A., Balsamo, G., Bauer, P., Bechtold, P., Beljaars, A. C. M., van de Berg, L., Bidlot, J., Bormann, N., Delsol, C., Dragani, R., Fuentes, M., Geer, A. J., Haimberger, L., Healy, S. B., Hersbach, H., Hólm, E. V., Isaksen, L., Kållberg, P., Köhler, M., Matricardi, M., McNally, A. P., Monge-Sanz, B. M., Morcrette, J.-J., Park, B.-K., Peubey, C., de Rosnay, P., Tavolato, C., Thépaut, J.-N., and Vitart, F.: The ERA-Interim reanalysis: configuration and performance of the data assimilation system, Q. J. Roy. Meteor. Soc., 137, 553–597, doi:10.1002/qj.828, 2011. 33735

Drdla, K. and Müller, R.: Temperature thresholds for chlorine activation and ozone loss in the polar stratosphere, Ann. Geophys., 30, 1055–1073, doi:10.5194/angeo-30-1055-2012, 2012. 33733, 33735, 33742

Fahey, D. W., Gao, R. S., Carslaw, K. S., Kettleborough, J., Popp, P. J., Northway, M. J., Holecek, J. C., Ciciora, S. C., McLaughlin, R. J., Thompson, T. L., Winkler, R. H., Baumgardner, D. G., Gandrud, B., Wennberg, R. O., Dhaniyala, S., McKinney, K., Peter, T., Salawitch, R. J., Bui, T. P., Elkins, J. W., Webster, C. R., Atlas, E. L., Jost, H., Wilson, J. C., Herman, R. L., Kleinböhl, A., and von König, M.: The detection of large HNO_3-containing particles in the winter Arctic stratosphere, Science, 291, 1026–1031, doi:10.1126/science.1057265, 2001. 33733

ACPD
15, 33731–33754, 2015

Gobbi, G. P.: Lidar estimation of stratospheric aerosol properties: surface, volume and extinction to backscatter ratio, J. Geophys. Res., 100, 11219–11235, doi:10.1029/94JD03106, 1995. 33735

Grooß, J.-U., Günther, G., Konopka, P., Müller, R., McKenna, D. S., Stroh, F., Vogel, B., Engel, A., Müller, M., Hoppel, K., Bevilacqua, R., Richard, E. an Webster, C. R., J. W. Elkins, Hurst, D. F., Romashkin, P. A., and Baumgardner, D. G.: Simulation of ozone depletion in spring 2000 with the Chemical Lagrangian Model of the Stratosphere (CLaMS), J. Geophys. Res., 107, 8295, doi:10.1029/2001JD000456, 2002. 33741

Grooß, J.-U., Engel, I., Borrmann, S., Frey, W., Günther, G., Hoyle, C. R., Kivi, R., Luo, B. P., Molleker, S., Peter, T., Pitts, M. C., Schlager, H., Stiller, G., Vömel, H., Walker, K. A., and Müller, R.: Nitric acid trihydrate nucleation and denitrification in the Arctic stratosphere, Atmos. Chem. Phys., 14, 1055–1073, doi:10.5194/acp-14-1055-2014, 2014. 33735

Junge, C. E., Chagnon, C. W., and Manson, J. E.: Stratospheric aerosols, J. Meteorol., 18, 81–108, 1961. 33732

Kelly, K. K., Tuck, A. F., Murphy, D. M., Proffitt, M. H., Fahey, D. W., Jones, R. L., McKenna, D. S., Loewenstein, M., Podolske, J. R., Strahan, S. E., Ferry, G. V., Chan, K. R., Vedder, J. F., Gregory, G. L., Hypes, W. D., McCormick, M. P., Browell, E. V., and Heidt, L. E.: Dehydration in the lower antarctic stratosphere during late winter and early spring, 1987, J. Geophys. Res., 94, 11317–11357, doi:10.1029/JD094iD09p11317, 1989. 33733

Kirner, O., Müller, R., Ruhnke, R., and Fischer, H.: Contribution of liquid, NAT and ice particles to chlorine activation and ozone depletion in Antarctic winter and spring, Atmos. Chem. Phys., 15, 2019–2030, doi:10.5194/acp-15-2019-2015, 2015. 33733

Kühl, S., Dörnbrack, A., Wilms-Grabe, W., Sinnhuber, B.-M., Platt, U., and Wagner, T.: Observational evidence of rapid chlorine activation by mountain waves above northern Scandinavia, J. Geophys. Res., 109, D22309, doi:10.1029/2004JD004797, 2004. 33733

Lambert, A., Santee, M. L., Wu, D. L., and Chae, J. H.: A-train CALIOP and MLS observations of early winter Antarctic polar stratospheric clouds and nitric acid in 2008, Atmos. Chem. Phys., 12, 2899–2931, doi:10.5194/acp-12-2899-2012, 2012. 33736

Livesey, N. J., Read, W. G., Froidevaux, L., Lambert, A., Manney, G. L., Pumphrey, H. C., Santee, M. L., Schwartz, M. J., Wang, S., Cofeld, R. E., Cuddy, D. T., Fuller, R. A., Jarnot, R. F., Jiang, J. H., Knosp, B. W., Stek, P. C., Wagner, P. A., and Wu., D. L.: Version 3.3 Level 2 data quality and description document, Technical Report JPL D-33509, Jet Propulsion

ACPD
15, 33731–33754, 2015

Laboratory, available at: https://mls.jpl.nasa.gov/data/v3-3_data_quality_document.pdf (last access: 27 November 2015), 2011. 33734

Lowe, D. and MacKenzie, A. R.: Polar stratospheric cloud microphysics and chemistry, J. Atmos. Sol.-Terr. Phy., 70, 13–40, 2008. 33732

McKenna, D. S., Konopka, P., Grooß, J.-U., Günther, G., Müller, R., Spang, R., Offermann, D., and Orsolini, Y.: A new Chemical Lagrangian Model of the Stratosphere (CLaMS): 1. Formulation of advection and mixing, J. Geophys. Res., 107, 4309, doi:10.1029/2000JD000114, 2002. 33735

Nash, E. R., Newman, P. A., Rosenfield, J. E., and Schoeberl, M. R.: An objective determination of the polar vortex using Ertel's potential vorticity, J. Geophys. Res., 101, 9471–9478, 1996. 33735, 33751

Pitts, M. C., Poole, L. R., and Thomason, L. W.: CALIPSO polar stratospheric cloud observations: second-generation detection algorithm and composition discrimination, Atmos. Chem. Phys., 9, 7577–7589, doi:10.5194/acp-9-7577-2009, 2009. 33733, 33734

Pitts, M. C., Poole, L. R., Dörnbrack, A., and Thomason, L. W.: The 2009–2010 Arctic polar stratospheric cloud season: a CALIPSO perspective, Atmos. Chem. Phys., 11, 2161–2177, doi:10.5194/acp-11-2161-2011, 2011. 33733, 33734, 33736, 33737

Pitts, M. C., Poole, L. R., Lambert, A., and Thomason, L. W.: An assessment of CALIOP polar stratospheric cloud composition classification, Atmos. Chem. Phys., 13, 2975–2988, doi:10.5194/acp-13-2975-2013, 2013. 33734, 33735

Portmann, R. W., Solomon, S., Garcia, R. R., Thomason, L. W., Poole, L. R., and McCormick, M. P.: Role of aerosol variations in anthropogenic ozone depletion in the polar regions, J. Geophys. Res., 101, 22991–23006, 1996. 33737, 33738

Rienecker, M. M., Suarez, M. J., Gelaro, R., Todling, R., Bacmeister, J., Liu, E., Bosilovich, M. G., Schubert, S. D., Takacs, L., Kim, G.-K., Bloom, S., Chen, J., Collins, D., Conaty, A., da Silva, A., Gu, W., Joiner, J., Koster, R. D., Lucchesi, R., Molod, A., Owens, T., Pawson, S., Pegion, P., Redder, C. R., Reichle, R., Robertson, F. R., Ruddick, A. G., Sienkiewicz, M., and Woollen, J.: MERRA: NASA's modern-era retrospective analysis for research and applications, J. Climate, 24, 3624–3648, doi:10.1175/JCLI-D-11-00015.1, 2011. 33735

Santee, M. L., Lambert, A., Read, W. G., Livesey, N. J., Manney, G. L., Cofield, R. R., Cuddy, D. T., Daffer, W. H., Froidevaux, L., Fuller, R. A., Jarnot, R. F., Knosp, B. W., Perun, V. S., Snyder, W. V., Stek, P. C., Thurstans, R. P., Wagner, P. A., Waters, J. W., Connor, B.,

ACPD
15, 33731–33754, 2015

Urban, J., Murtagh, D., Ricaud, P., Barret, B., Kleinböhl, A., J, K., Küllmann, H., von Hobe, M., Toon, G. C., and Stachnik, R. A.: Validation of the aura microwave limb sounder ClO measurements, J. Geophys. Res, 113, D15S22, doi:10.1029/2007JD008762, 2008. 33734

Solomon, S.: Stratospheric ozone depletion, a review of concepts and history, Rev. Geophys., 37, 275–316, 1999. 33732

Solomon, S., Garcia, R. R., Rowland, F. S., and Wuebbles, D. J.: On the depletion of Antarctic ozone, Nature, 321, 755–758, 1986. 33733

Stephens, G. L., Vane, D., Boain, R., Mace, G., Sassen, K., Wang, Z., Illingworth, A., O'Connor, E., Rossow, W., Durden, S., Miller, S., Austin, R., Benedetti, A., Mitrescu, C., and Team, C. S.: The CloudSat mission and the A-Train: a new dimension of space-based observations of clouds and precipitation, B. Am. Meteorol. Soc., 83, 1771–1790, doi:10.1175/BAMS-83-12-1771, 2002. 33734

Waters, J. W., Froidevaux, L., Harwood, R. S., Jarnot, R. F., Pickett, H. M., Read, W. G., Siegel, P. H., Cofield, R. R., Filipak, M. J., Flower, D. A., Holden, J. R., Lau, G. K., Livesey, N. J., Manney, G. L., Pumphrey, H. C., Santee, M. L., Wu, D. L., Cuddy, D. T., Lay, R. R., Loo, M. S., Perun, C. S., Schwartz, M. J., Stek, P. C., Thurstans, R. P., Boyles, M. A., Chandra, K. M., Chavez, M. C., Chen, G.-S., Chudasama, B. V., Dodge, R., Fuller, R. A., Girard, M. A., Jiang, J. H., Jiang, Y., Knosp, B. W., LaBelle, R. C., Lam, J. C., Lee, K. A., Miller, D., Oswald, J. E., Patel, N. C., Pukala, D. M., Quintero, O., Scaff, D. M., Snyder, W. V., Tope, M. C., Wagner, P. A., and Walch, M. J.: The Earth Observing System Microwave Limb Sounder (EOS MLS) on the Aura satellite, IEEE T. Geosci. Remote, 44, 1075–1092, doi:10.1109/TGRS.2006.873771, 2006. 33734

Wegner, T., Grooß, J.-U., von Hobe, M., Stroh, F., Sumińska-Ebersoldt, O., Volk, C. M., Hösen, E., Mitev, V., Shur, G., and Müller, R.: Heterogeneous chlorine activation on stratospheric aerosols and clouds in the Arctic polar vortex, Atmos. Chem. Phys., 12, 11095–11106, doi:10.5194/acp-12-11095-2012, 2012. 33733

Winker, D. M., Vaughan, M. A., Omar, A., Hu, Y., Powell, K. A., Liu, Z., Hunt, W. H., and Young, S. A.: Overview of the CALIPSO Mission and CALIOP data processing algorithms, J. Atmos. Ocean. Tech., 26, 2310–2323, doi:10.1175/2009JTECHA1281.1, 2009. 33734

Wohltmann, I., Wegner, T., Müller, R., Lehmann, R., Rex, M., Manney, G. L., Santee, M. L., Bernath, P., Sumińska-Ebersoldt, O., Stroh, F., von Hobe, M., Volk, C. M., Hösen, E., Ravegnani, F., Ulanovsky, A., and Yushkov, V.: Uncertainties in modelling heterogeneous chemistry

ACPD
15, 33731–33754, 2015

and Arctic ozone depletion in the winter 2009/2010, Atmos. Chem. Phys., 13, 3909–3929, doi:10.5194/acp-13-3909-2013, 2013. 33733, 33742

ACPD
15, 33731–33754, 2015

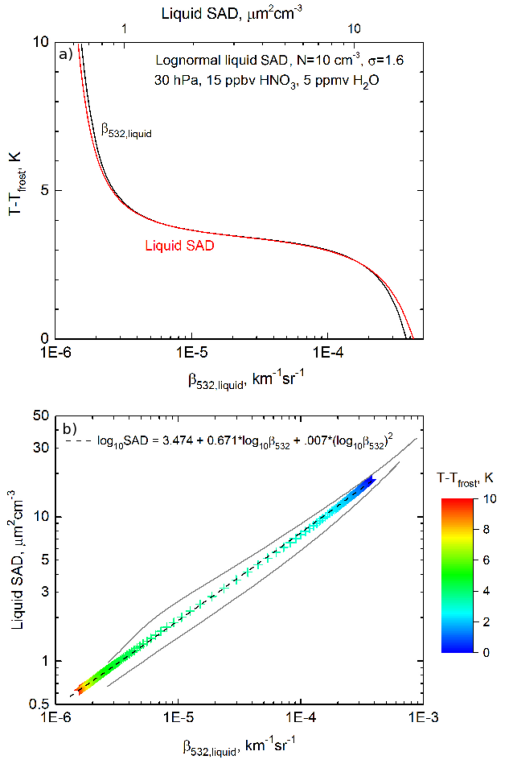

Figure 1. (a) Temperature dependence of STS surface area density and the corresponding theoretical backscatter signal at 532 nm for typical stratospheric conditions. **(b)** Relationship between STS surface area density and particulate backscatter color coded according to their theoretical temperature. Gray curves mark the deviation from the fitted function for varying ambient conditions.

ACPD
15, 33731–33754, 2015

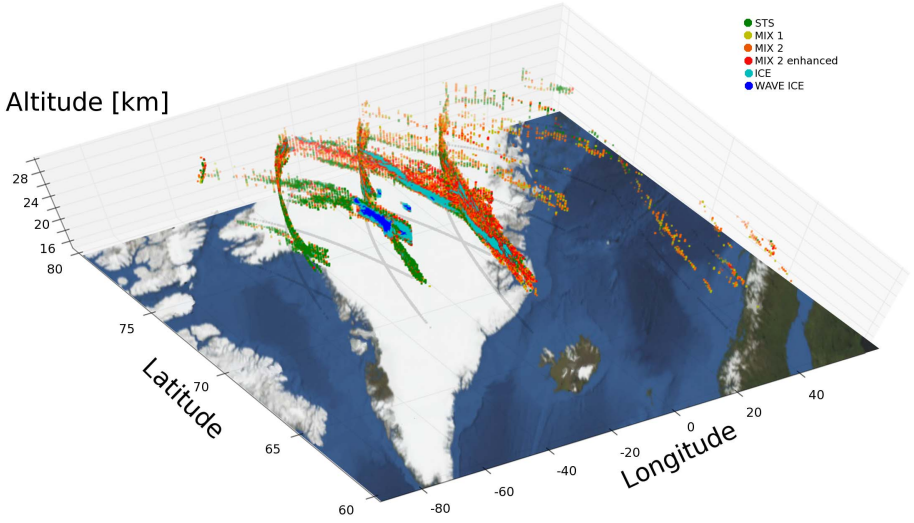

Figure 2. CALIOP PSC observations along orbits over Greenland on 2 January 2010 color coded according to the CALIOP classification. Green: STS; Yellow: MIX 1; Orange: MIX 2; Red: MIX 2 enhanced; Cyan: Synoptic Ice; Blue: Wave Ice.

ACPD
15, 33731–33754, 2015

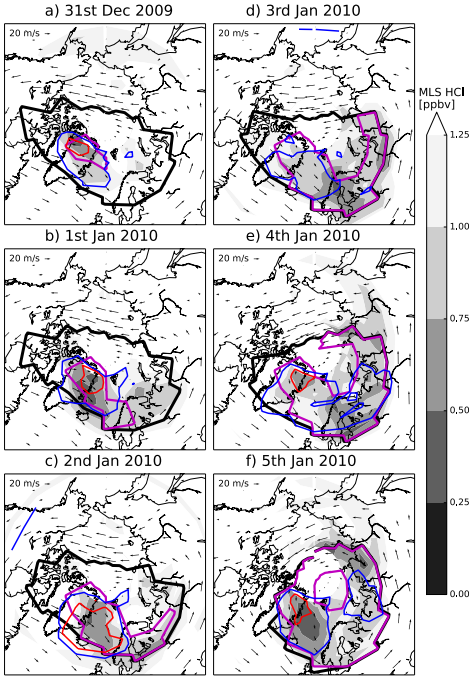

Figure 3. The meteorological situation on six days for the Arctic winter 2009/2010 on the 510 K isentrope (approximately 22 km). Arrows show the prevailing wind direction and speed. The vortex edge is calculated according to Nash et al. (1996) and shown in solid black. Solid magenta indicates regions of the vortex where air which has passed through a PSC is present. Blue and red contours show the particulate backscatter from CALIOP where blue represents the detection limit for CALIOP (3×10^{-5} km^{-1} sr^{-1}) and red values indicative of PSCs with a surface area density of more than 10 times the background values (1.5×10^{-4} km^{-1} sr^{-1}). Grey contours show HCl mixing ratios from MLS.

ACPD
15, 33731–33754, 2015

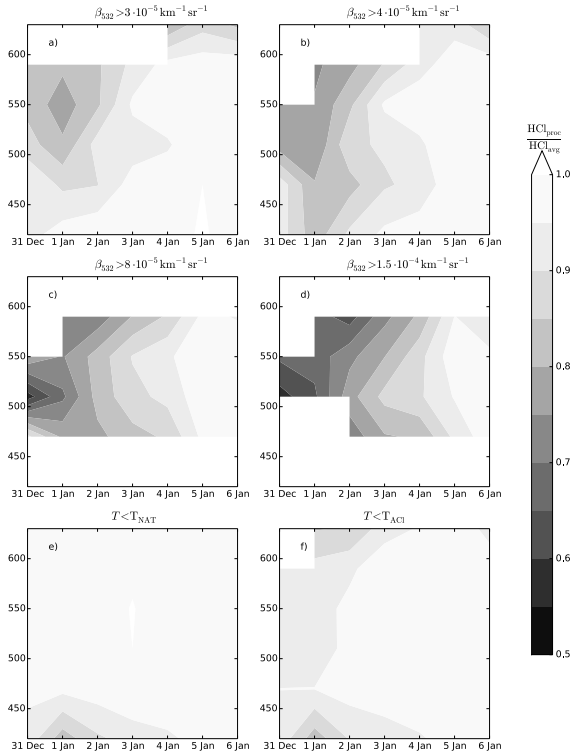

Figure 4. Ratio of average HCl mixing ratio of air that passed through a specified area to the vortex average HCl mixing ratio. The ratio is calculated for six areas, four encompassed by backscatter thresholds **(a–d)** and two by temperature thresholds **(e, f)**. A ratio of less than one indicates air inside the contour has a lower HCl mixing ratio than the vortex average.

ACPD
15, 33731–33754, 2015

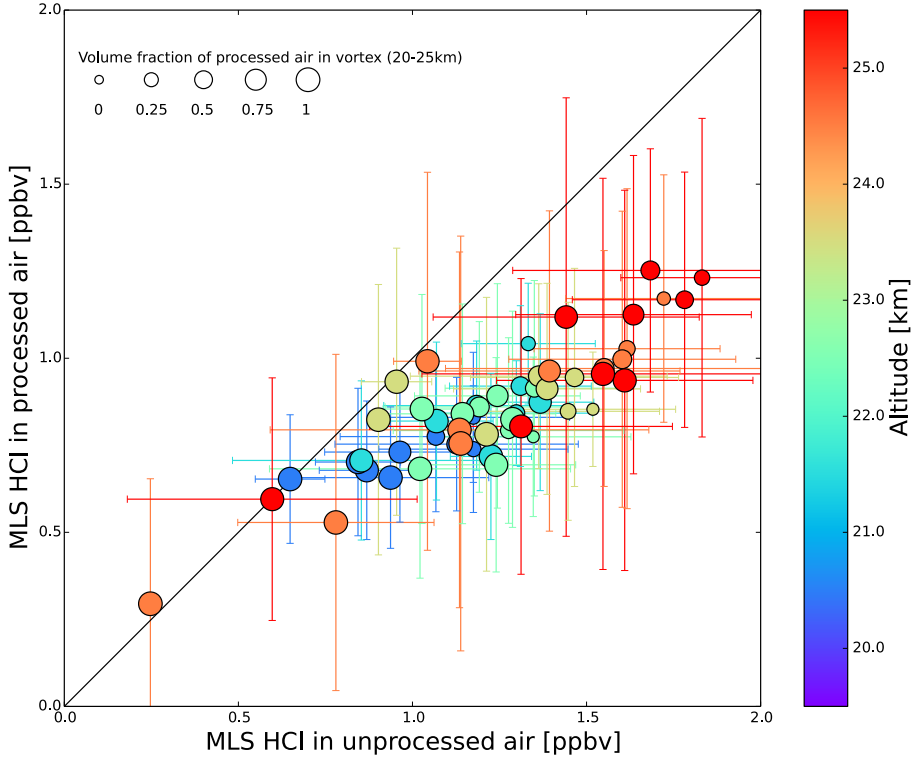

Figure 5. Correlation of daily average MLS HCl in processed and unprocessed air from 31 December 2009 to 9 January 2010 for six different altitudes. Error bars indicate the 1-σ standard deviation of calculating the daily average HCl mixing ratios.

ACPD
15, 33731–33754, 2015

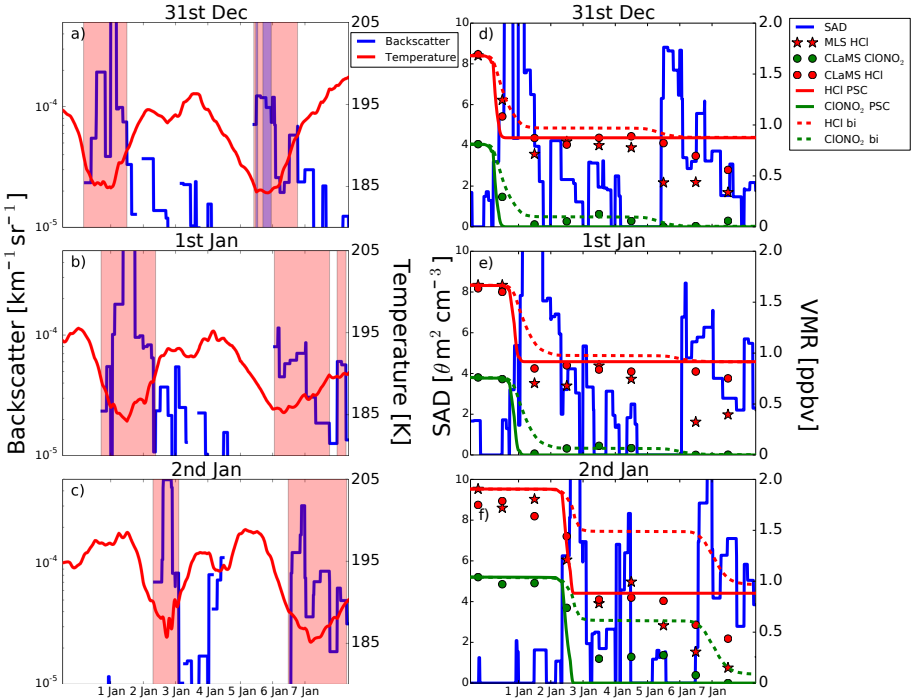

Figure 6. Temporal evolution of trajectories intersecting with the backscatter maximum on three different days on 510 K potential temperature. Left column shows backscatter (blue), temperature (red), time below $T_{NAT} - 3$ K (red shading) and time below T_{ICE} (blue shading). Right column shows surface area density (blue), HCl (red) and $ClONO_2$ (green). Red stars are the daily mean HCl mixing ratios observed by MLS interpolated on the position of the trajectory and circles are CLaMS mixing ratios of HCl (red) and $ClONO_2$ (green), respectively. Solid red and green lines represent HCl and $ClONO_2$ where SAD for calculating heterogeneous reaction rates is calculated from the observed backscatter. Dashed red and green lines represent HCl and $ClONO_2$ where SAD is calculated for a binary aerosol.

ACPD
15, 33731–33754, 2015